Published in final edited form as:

J Am Chem Soc. 2023 January 18; 145(2): 1072–1082. doi:10.1021/jacs.2c10672.

Enhancing Dynamic Spectral Diffusion in Metal-Organic Frameworks Through Defect Engineering

Arjun Halder[a], **David C. Bain**[a], **Julia Oktawiec**[b], **Matthew A. Addicoat**[c], **Stavrini Tsangari**[a], **José J. Fuentes-Rivera**[a], **Tristan A. Pitt**[a], **Andrew J. Musser**[a,*], **Phillip J. Milner**[a,*]

[a]Department of Chemistry and Chemical Biology, Cornell University, Ithaca, NY, 14850, United States

[b]Department of Chemistry, Northwestern University, Evanston, IL, 60208, United States

[c]School of Science and Technology, Nottingham Trent University, Clifton Lane, NG11 8NS, Nottingham, United Kingdom

Abstract

The crystal packing of organic chromophores has a profound impact on their photophysical properties. Molecular crystal engineering is generally incapable of producing precisely spaced arrays of molecules for use in photovoltaics, light-emitting diodes, and sensors. A promising alternative strategy is the incorporation of chromophores into crystalline metal-organic frameworks (MOFs), leading to matrix coordination-induced emission (MCIE) upon confinement. However, it remains unclear how the precise arrangement of chromophores and defects dictates photophysical properties in these systems, limiting the rational design of well-defined photoluminescent materials. Herein, we report new, robust Zr-based MOFs constructed from the linker tetrakis(4-carboxyphenyl)ethylene ($TCPE^{4-}$) that exhibit an unexpected structural transition in combination with a prominent shift from green to blue photoluminescence (PL) as a function of the amount of acid modulator (benzoic, formic, or acetic acid) used during synthesis. Time-resolved PL (TRPL) measurements provide full spectral information and reveal that the observed hypsochromic shift arises due to a higher concentration of linker substitution defects at higher modulator concentrations, leading to broader excitation transfer-induced spectral diffusion. Spectral diffusion of this type has not been reported in a MOF to date, and its observation provides structural information that is otherwise unobtainable using traditional crystallographic techniques. Our findings suggest that defects have a profound impact on the photophysical properties of MOFs, and that their presence can be readily tuned to modify energy transfer processes within these materials.

Graphical Abstract

*Corresponding Author ajm557@cornell.edu, pjm347@cornell.edu.

Supporting Information. Characterization data and details of all experiments. This material is available free of charge via the Internet at http://pubs.acs.org.

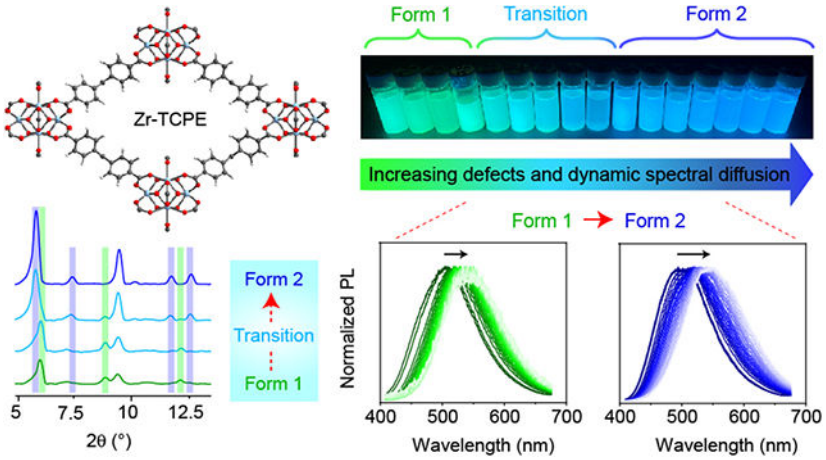

Introduction.

Photoactive organic molecules form the basis of numerous technologies, including light-harvesting and generation,[1] photocatalysis,[2,3] and sensing.[4-7] However, tuning the photophysical properties of chromophores—especially in the solid state—remains a long-standing challenge in the field. Such properties are highly dependent on the local packing of molecules, which is traditionally difficult to control in crystals held together by weak intermolecular forces. Therefore, rationally tuning the photophysical properties of organic molecules, such as emission wavelength and excited-state lifetime, represents a barrier to the design of new photoactive materials. Simple strategies for overcoming this limitation could pave the way for next-generation materials such as stable blue-emitting organic light-emitting diodes (OLEDs),[8] among many others.

The confinement of chromophores within metal-organic frameworks (MOFs) provides an intriguing platform for overcoming these challenges by enabling programmable control over their local environment in the solid state.[1,9-15] For example, MOFs present an alternative to aggregation-induced emission (AIE) as a means to “turn on” the photoluminescence of tetraphenylethylene (TPE) derivatives through matrix coordination-induced emission (MCIE).[16-19] However, precisely tuning the photophysical properties of chromophores confined within MOFs still presents several challenges. First, altering the local environment of a chromophore generally requires changing the organic linker, metal node, and/or underlying framework topology, all of which can have a dramatic (and unpredictable) effect on photophysical properties.[1,10] In addition, the need to avoid quenching or metal-based luminescence limits the choice of metals suitable for preparing MOFs displaying linker-based emission.[20] Last, many photoluminescent MOFs degrade or suffer from quenched fluorescence upon exposure to water, limiting their application under realistic conditions.[21-25] Ideally, one would be able to dial in the desired photophysical properties of a chromophore confined within a stable MOF, streamlining the preparation of new photoluminescent materials with tailorable properties.

Defect engineering enables the introduction of new local environments within MOFs without changing their bulk structures.[26-36] Generally, defect sites are inserted by

coordination modulation, in which a monodentate competitor for the linker is added during MOF synthesis, leading to missing linker and/or node defects.[26,27] In particular, Zr-based frameworks exhibit high tolerance towards defects due to their highly interconnected structures.[36-38] Although defect engineering is widely employed to improve the catalytic activity,[39] gas binding affinity,[35] and porosity[30] of MOFs, its application for tuning MOF photophysical properties remains relatively unexplored.[40]

Herein, we demonstrate that the controlled introduction of defects within photoluminescent MOFs enables modification of their intrinsic photophysical properties. In particular, upon increasing the concentration of added formic acid (FA), acetic acid (AA), or benzoic acid (BA) during the synthesis of the new framework CORN-MOF-5 (CORN = Cornell University), referred to herein as Zr-TCPE ($TCPE^{4-}$ = tetrakis(4-carboxyphenyl)ethylene), we observe a distinct structural transition (Form 1 to Form 2) without a change in the underlying **scu** topology. This structural change coincides with an increase in linker substitution defects in Form 2, which contributes to a pronounced shift from green to blue photoluminescence (PL). Time-resolved PL (TRPL) spectroscopy measurements reveal that this greater density of defect sites in Form 2 leads to distinctive excitation transfer-induced spectral diffusion and the observed blue shift in its steady-state PL profile, along with smaller contributions from differences in intermolecular coupling. Dynamic spectral diffusion of this type has not been observed in MOFs to date and provides key insights into the interplay between defect concentration and photophysical properties that underpin the properties of photoactive MOFs. Overall, our findings reveal that defect engineering represents a straightforward strategy for modifying the local environment of photoactive molecules under confinement and that photophysical measurements offer a new handle for probing the nature of defect sites within photoluminescent MOFs.

Result and Discussion.

Derivatives of TPE have been shown to undergo AIE due to restriction of intramolecular motions of the phenyl rings or the existence of a conical intersection in the solid state.[41-45] Because TPE derivatives are AIE-active and a rigid MOF can activate photoluminescence of TPEs via MCIE,[18,19] we aimed to study the effect of defects on photophysical properties using a $TCPE^{4-}$-based MOF as a model system (see Supporting Information or SI Section 2a-b for synthetic details). This linker has been previously employed to prepare frameworks from Zn,[18,25] Cd,[18] La, Nd,[24] and UO_2,[22,23] but its incorporation into a Zr-based MOF (with **she** topology) was only reported during the preparation of this manuscript.[46] A series of Zr-TCPE MOFs were initially synthesized at 120 °C for 48 h using $ZrCl_4$ as a metal precursor, formic acid (FA) as a modulator, H_2O to facilitate Zr_6 cluster formation, and *N*,*N*-dimethylformamide (DMF) as a solvent (Figure 1a, SI Section 2c). Varying equivalents (0–200 equiv.) of FA were employed in order to elucidate the effect of modulator concentration on framework photophysics. After synthesis, the MOFs were extensively soaked in DMF and methanol or tetrahydrofuran to remove soluble impurities prior to drying in air and characterization by powder X-ray diffraction (PXRD) as well as attenuated total reflectance infrared (ATR-IR) spectroscopy, 77 K N_2 adsorption measurements, thermogravimetric analysis (TGA), and scanning electron microscopy (SEM) in select cases (SI Sections 3-5).

Herein, MOF samples are termed Zr-TCPE-FA(x), where x represents the equivalents of FA utilized compared to H_4TCPE.

Crystalline Zr-TCPE MOFs were obtained under all tested conditions. Unexpectedly, a phase transition as a function of modulator equivalents was observed by PXRD in the Zr-TCPE samples (Figure 1b). The PXRD patterns corresponding to samples prepared with low (0–80) and high (125–200) equivalents of FA are similar but distinct in the low angle regime (<15° 2θ), with a mixture of phases observed at intermediate equivalents of FA (90–100). Herein, we designate the two phases of the MOF Form 1 and Form 2. These patterns also diverge from that of the TCPE-based MOF reported with **she** topology (SI Figure S48); These patterns also diverge from that of the TCPE-based MOF reported with she topology (SI Figure S48); the divergent topologies for Zr-TCPE frameworks are likely due to the different Zr precursors and modulators used herein ($ZrCl_4$ and FA/AA/BA) compared to previous work ($ZrOCl_2$ and trifluoroacetic acid).[46] Nonetheless, the comparable SEM images of Zr-TCPE-FA(50) and Zr-TCPE-FA(200), representative samples of Form 1 and Form 2, respectively, confirm that the two phases are likely topologically similar (SI Figure S26). For Form 1, a gradual broadening of the reflections due to a decrease in crystallinity was observed above 50 equiv., which is not expected given the increase in crystallinity that is generally observed when higher equivalents of acid modulators are employed.[26,30,36] In contrast, the crystallinity of Form 2 increased with increasing equivalents of FA, as expected. Because the role of acid modulators is generally to enhance the reversibility of MOF formation,[26] we hypothesize that Form 1 is a kinetic phase whereas Form 2 is the thermodynamically favored phase. Consistently, post-synthetic treatment of Form 1 with excess FA converted it to Form 2, as confirmed by PXRD (SI Figure S29). Notably, changes in the Zr-MOF phase as a function of modulator concentration are relatively rare and generally involve more dramatic shifts in the underlying framework topology.[47]

Despite significant effort, single crystals of either phase of Zr-TCPE could not be obtained. To gain insight into the most likely structures of Form 1 and Form 2, we simulated plausible structures using AuToGraFS[48] that were further optimized using UFF4MOF[49,50] as implemented in a development version of AMS 2020 (SI Section 8).[51] The combination of Zr_6 nodes and 4-connected linkers ($TCPE^{4-}$) can potentially crystallize in **csq** (akin to PCN-128),[52] **scu** (akin to NU-901),[53] **ftw** (akin to PCN-94),[54] or **she** topologies.[46] For **csq** and **scu** topologies, there are two possible orientations of the $TCPE^{4-}$ linkers relative to the largest pore aperture, with the alkenes either parallel or perpendicular to the pore direction (SI Figures S45-S46). The simulated patterns corresponding to structures with **scu** topologies matched most closely to the experimental PXRD patterns of Zr-TCPE-FA(50) and Zr-TCPE-FA(200) and were chosen for further examination (SI Figures S47). Notably, Pawley refinement using the unit cell parameters corresponding to the reported Zr-TCPE MOF with **she** topology led to poor fits to the experimental data for both Forms, confirming that they are topologically distinct (SI Figures S14-15).[46]

Indexing and Rietveld refinement of the experimental patterns were carried out to obtain potential structural models for both forms of Zr-TCPE. For the more crystalline Form 2, further optimization of the initial **scu** structure and the addition of two bidentate formate molecules per cluster produced an orthorhombic structure (Zr_6 (μ_3-O)$_4$(μ_3-

$OH)_4(HCO_2)_2(TCPE)_2(OH)_2(H_2O)_2$) in the *Cmmm* space group with a = 30.34(17) Å, b = 17.50(7) Å, and c = 12.00(3) Å (Figure 2c, d; SI Section 3).[55] The simulated PXRD pattern corresponding to this structure closely matches the experimental pattern of Zr-TCPE-FA(200), as confirmed by Rietveld refinement (Figure 2e; SI Figure S12).

The modest crystallinity of Form 1, which is likely due to reduced reaction reversibility when lower amounts of acid modulators are employed, made structure elucidation more challenging. Consistently, the 77 K N_2 Brunauer–Emmett–Teller (BET) surface area of Zr-TCPE-FA(30) (270 ± 1 m^2/g) is lower than that of Zr-TCPE-FA(200) (1013 ± 2 m^2/g) (SI Figures S17, S24). We hypothesize that the higher surface area of Zr-TCPE-FA(200) is due to its higher crystallinity and larger extent of mesopores, as suggested by density functional theory (DFT) pore size distribution calculations (SI Figure S24). Indexing the experimental PXRD pattern of Zr-TCPE-FA(50) suggested an orthorhombic solution in the *Pmma* space group with a = 16.77(16) Å, b = 12.26(20) Å and c = 30.03(4) Å (SI Section 3). The closest-matching structural model to Form 1 corresponds to a modified Form 2 structure with a molecular formula of $Zr_6(\mu_3\text{-}O)_4(\mu_3\text{-}OH)_4(TCPE)_2(OH)_4(H_2O)_4$ in which some of the linkers change orientation relative to the large pore dimension (Figure 2a, b). Rietveld refinement (SI Figure S11) confirms that this model displays a better fit to the experimental data than the structural model for Form 2 (SI Figure S13). Together, these structural models indicate that Zr-TCPE undergoes a subtle but distinct transition in the relative linker orientations as a function of modular concentration.

To investigate the generality of this phenomenon, Zr-TCPE frameworks were prepared with two other modulators, acetic acid (AA) and benzoic acid (BA) (Figure 3, SI Sections 2 and 4). These frameworks are designated Zr-TCPE-AA(x) and Zr-TCPE-BA(x), respectively, where x represents the equivalents of AA or BA utilized compared to H_4TCPE. Varying equivalents (0–200 equiv. for AA and 0–100 equiv. for BA) of both modulators were evaluated without changing any other synthetic parameters. Intriguingly, the same switch from Form 1 to Form 2 as a function of modulator concentration was observed in both cases (Figure 3, SI Figure S49). For AA, the transition from Form 1 to Form 2 occurred at lower equivalents of modulator (60 equiv., Figure 3) than with FA (90–100 equiv., Figure 1). This is likely because AA is a better competitor with the linker for the Zr nodes, making MOF formation more reversible.[26,30] Consistently, BA induced the phase change at the lowest concentration (30 equiv.) among tested modulators, reflecting its general superiority as a modulator for the synthesis of Zr-MOFs.[26,28] Both Zr-TCPE-AA(200) and Zr-TCPE-BA(100) could be obtained with high crystallinity. The 77 K N_2 BET surface areas of Zr-TCPE-AA(200) and Zr-TCPE-BA(100) were determined to be 979 ± 2 and 1102 ± 5 m^2/g, respectively (SI Figure S17), similar to that of Zr-TCPE-FA(200) (1013 ± 2 m^2/g). The N_2 uptake of Zr-TCPE-BA(100) at higher pressures of N_2 ($P/P_0 > 0.5$) was significantly higher than that of the other two MOFs, indicative of significant missing linker defects (see below).[28] Overall, these results suggest that monocarboxylic acid modulators generally induce a phase transition from Form 1 to Form 2 in Zr-TCPE MOFs with **scu** topologies.

Because rigidification within MOFs can activate the PL of TPE derivatives, we next investigated the photophysical properties of all synthesized Zr-TCPE MOFs (SI Section 7).[12,18,54,56] First, Zr-TCPE samples were suspended in dichloromethane (1 mg/mL) and

irradiated with UV light, allowing for direct visualization of the shift in PL maximum as a function of modulator equivalents (Figure 4a-c). Intriguingly, a clear transition from green emission for Form 1 to cyan emission for mixtures of phases to blue emission for Form 2 could be observed for FA- and BA-modulated samples, with a more gradual transition observed for AA-modulated samples.[18] Likewise, the emission color of Zr-TCPE-AA(200) is not as deep blue as that of samples prepared with high concentrations of FA and BA (see below for discussion). The PL spectra of Zr-TCPE-FA(50) and Zr-TCPE-FA(200) suspended in solvents of varying polarity were nearly identical, indicating that the emission properties of Zr-TCPE frameworks are largely solvent independent (SI Figures 36-37). Importantly, the crystallinity and PL intensity of Zr-TCPE-FA(50) and Zr-TCPE-FA(200) were also retained after suspension in water for 48 h, indicating that these materials are promising for applications under aqueous conditions (Figure S28).[46,57-59]

In order to elucidate the origins of the unexpected shift in emission color as a function of phase and modulator equivalents, steady-state PL spectra of all samples were first collected (Figure 4d-f). The maximum PL emission wavelength of all samples was similar to that of H_4TCPE (524 nm), supporting that linker-based emission dominates in these materials. Upon excitation at 355 nm, a pronounced hypsochromic shift in the PL maximum was observed with higher equivalents of all three modulators. Intriguingly, the shifts in emission wavelength largely line up with the phase change from Form 1 to Form 2 observed by PXRD. For example, the maximum emission wavelength with low equivalents of modulator (Form 1) is 510 nm (green fluorescence), whereas emission near 490 nm (blue fluorescence) is observed with higher equivalents of modulator (Form 2). This transition is more dramatic for FA and BA than for AA (see below for discussion). Consistent with the assignment of green emission corresponding to Form 1 and blue emission corresponding to Form 2, post-synthetic treatment of Zr-TCPE-FA(30) with FA led to a switch from Form 1 to Form 2 concomitant with a change in the PL from green to blue emission (SI Figures 29-30).

To better understand the structural origins of the observed shift in PL emission as a function of modulator concentration in Zr-TCPE MOFs, we carried out PL excitation and time-resolved photoluminescence (TRPL) measurements. PL excitation maps (SI Figures S33-S35) provide similar information to standard diffuse reflectance UV-Vis absorbance spectra but with less dependence on sample crystallinity and morphology. These spectra confirm that the UV-Vis absorption features of all Zr-TCPE MOFs are linker-based and largely unaffected by the nature of the modulator employed (see SI Section 7 for further discussion). This finding supports that the observed change in emission wavelength is due to an excited state phenomenon and not due to changes in the ground states of Zr-TCPE materials.

The nature of the excited states of the two phases of Zr-TCPE MOFs were probed using nanosecond TRPL spectroscopy (Figure 5). We employed an intensified charge-coupled device (iCCD) camera capable of resolving full spectral evolution with 480 ps resolution. This technique provides important information about excited state dynamics that is not easily obtainable using single wavelength techniques such as time-correlated single photon counting (TCSPC) or photodiode detection techniques.[60,61] In TRPL measurements, many sequential spectra are collected immediately after photoexcitation of the MOF using a 355

nm pulsed laser, providing snapshots of the MOF emission spectrum at specific time points as the photoexcited state decays. Figure 5a-b display the normalized spectral evolution of Zr-TCPE-FA(50) and Zr-TCPE-FA(200) as representative samples of Form 1 and Form 2, respectively, obtained from the TRPL measurements. Over the first 37.5 ns, there is a uniform shift of the emission spectrum to lower energies. This phenomenon has previously been termed spectral diffusion in the field of organic solids and is a manifestation of energy transport within disordered systems.[62-67] For Form 1, the peak maximum shifts by 29 nm (504 nm to 533 nm), while in Form 2, the peak shifts by 55 nm (494 nm to 549 nm), which is nearly double. These findings confirm that the degree of spectral diffusion is greater in Form 2 than in Form 1.

The enhanced spectral diffusion in Form 2 indicates that there is a broader density of emitting states, which in turn leads to its higher energy emission (blue fluorescence) compared to Form 1 (green fluorescence). The color of the MOFs' fluorescence by eye is experimentally reflected in their steady-state fluorescence spectra. The steady-state fluorescence can be thought of as a time-weighted average of all the TRPL spectra with the earlier time spectra carrying more weight in the resulting steady-state spectrum due to their higher intensities.[68] For these MOFs, particularly in Form 2, a larger spectral shift in the TRPL measurement results in a more blue-shifted spectrum with a more skewed spectral shape in the steady-state.[62] It should be noted that this is the first time spectral diffusion of this nature has been observed in a MOF.

The TRPL data discussed above lead to two critical questions: what is the origin of spectral diffusion in Zr-TCPE MOFs, and why does Form 2 display more pronounced spectral diffusion than Form 1? There are two general mechanisms for spectral diffusion, which can be described in terms of physical motion of the excitation as either static or dynamic.[69] In static spectral diffusion, the MOF structure would distort upon photoexcitation and the photoexcited site would subsequently relax to a more favorable geometry as emission occurs. In dynamic spectral diffusion, the MOF structure would be static, but excitations would hop around the MOF lattice from linker to linker to reach lower energy sites. Both processes would produce a spectral shift over time in a TRPL measurement and can occur simultaneously or on different timescales. The two processes can be distinguished by their dependence on excitation wavelength. In a static picture, the degree of spectral shift is controlled by the degree of structural relaxation possible in the system. This is typically set by the local bonding structure and intermolecular interactions and should be independent of excitation wavelength. The excess energy imparted by high-energy excitation in such a model is typically dissipated through thermalization much faster than the nanosecond timescales reported here. On the other hand, a dynamic model presupposes a broad density of states, in which each excitation wavelength selects a different ensemble. As long as the low-energy sites are similarly accessible, we would expect a progressively greater degree of shift for shorter excitation wavelengths.

To determine the type of spectral diffusion occurring in Zr-TCPE MOFs, we characterized the spectral diffusion in these materials as a function of excitation wavelength (Figure 5c-d). For both Form 1 and 2, the significant excitation dependence of the spectral shift is consistent with dynamic spectral diffusion. Furthermore, the spectral diffusion (monitored

by peak maximum over time) follows a logarithmic dependence as a function of time, which is also expected for dynamic spectral diffusion.[62,65,67] As expected, the degree of spectral diffusion is greater in Form 2 than in Form 1.

The PL anisotropy measurements and spectral decay profiles derived from the TRPL measurements provide further support for dynamic spectral diffusion in Zr-TCPE MOFs. In PL anisotropy measurements, the excitation source is vertically polarized to only excite dipoles that are aligned in that direction. If the dipoles change orientation via hopping (dynamic spectral diffusion), then the anisotropy will decay to zero as dipole angles become randomized. On the other hand, if excitations are localized on the rigid MOF (static spectral diffusion), then the anisotropy should not decay and will be fixed at 0.4.[69-71] We find the anisotropy is already zero within the time resolution of the measurement (SI Figures S38-S39). Hence, there must be excitation hopping, further supporting that dynamic spectral diffusion is occurring in these materials. In fact, there must be some extent of hopping faster than the 480 ps time resolution of our experiment, along with the observed ns timescale spectral diffusion. Such fast hopping times are to be expected in such a condensed-phase system, but the rate highly depends on the distance and overlap between chromophores as well as the nature of the coupling between them.[72-74] In addition, the PL intensity decay profiles are clearly nonexponential for both TCPE-FA(50) and TCPE-FA(200) (SI Figures S40-S41) and can be fitted to a stretched exponential indicative of a trapping model for the excitations (SI Figure S41, see SI Section 7 for details).[75] In this model, excitation hopping samples various sites in the MOF lattice, where it will eventually relax radiatively or get trapped at a defect site and decay non-radiatively. This model makes it difficult to assign a number to the lifetime of the excited state, but visual inspection of the decay curve shows that it lasts for >30 ns (see SI Section 7). Overall, the PL data confirm that the green to blue fluorescence shift observed in conjunction with the phase transition from Form 1 to Form 2 arises from the broadened density of emitting states and enhanced dynamic spectral diffusion in Form 2 compared to Form 1.

More pronounced spectral diffusion in materials prepared with high concentrations of acid modulators indicates that these materials possess a wider range of excited states compared to materials prepared with less acid modulator. That is, they are more photophysically disordered despite possessing higher crystalline order. We hypothesized that this is likely due to an increase in missing linker defects—in which linkers are substituted for the modulator conjugate base—when more modulator is used during MOF synthesis.[26,30] To support this hypothesis, Zr-TCPE-FA MOFs prepared using a range of FA concentrations were subject to chemical digestion to determine the ratios of formate to $TCPE^{4-}$ in each sample (Figure 6a). From ^{1}H NMR analysis of the digested samples, a gradual increase in the formate:$TCPE^{4-}$ ratio was observed for Form 1, with a sharp increase in formate concentration in Form 2 (Figure 6a). The higher degree of defect incorporation in Form 2 compared to Form 1 is likely due in part to the improved thermodynamic stability of Form 2, which increases its defect tolerance. Notably, the same trend was observed upon digestion of representative samples of Form 1 and Form 2 of Zr-TCPE-AA and Zr-TCPE-BA as well, in accordance with the PL results (Figure 6b). Further, the degree of defect incorporation for AA is less than that for FA and BA, which likely explains the less dramatic shift in PL color for Zr-TCPE-AA samples compared to Zr-TCPE-FA and Zr-TCPE-BA (Figure 4). Together,

the correlation between enhanced defect incorporation—leading to more dynamic spectral diffusion—and a blue shift in the PL emission wavelength of Zr-TCPE MOFs confirms that defect engineering represents a simple strategy for modifying the photophysical features of chromophores confined in MOFs. It is worth noting that the detailed information obtained from the spectroscopic measurements is not obtainable using traditional X-ray diffraction techniques, as the defects do not seem to exhibit long-range order in these materials.

These results together present a counter-intuitive picture. Typically, defects in condensed-phase molecular materials are associated with lower energy states and red-shifted emission, whereas the more defect-rich Form 2 here emits at distinctly higher average energies. This effect is the result of a subtle interplay between the defect-induced density of states and the rate of relaxation through it. Close examination of the results in Figure 5 reveals that while Form 2 emits at higher energy on average, it also exhibits dynamic spectral shifts to lower energy states than are present in Form 1. That is, the higher density of defects in Form 2 results in a broadening of the density of emitting states to higher and lower energies, as would be expected. However, the rate of relaxation through this manifold is relatively slow, likely due to the predominantly dipole-dipole-mediated coupling between chromophores and the relatively large separation between TPE units. Thus, radiative and non-radiative excited-state deactivation largely depletes the population before it reaches the low-energy defects, resulting in the average emission being dominated by the high-energy states populated earliest in the relaxation pathway.

Conclusion.

In summary, we have showcased how to simply and strategically control TPE emission wavelength through defect engineering for the first time in Zr-MOFs. By varying modulator concentration during MOF synthesis, Zr-TCPE crystallizes in two distinct phases (Form 1 and Form 2), likely due to a change in the preferred linker orientation during MOF formation. The phase change coincides with a higher concentration of linker substitution defects at higher modulator concentrations, which in turn leads to enhanced dynamic spectral diffusion and a blue-shift in the emission spectrum. Our findings highlight that small changes in defect concentration play a crucial role in regulating energy transfer and emission properties within MOFs. These findings must be considered when developing next-generation MOF-based photocatalysts and light-harvesting/emitting materials that rely on energy transfer or charge transfer processes. In addition, our observation of dynamic spectral diffusion in MOFs for the first time using TRPL measurements highlights the promise of this technique for uncovering complex photophysical pathways in photoluminescent frameworks.

Supplementary Material

Refer to Web version on PubMed Central for supplementary material.

ACKNOWLEDGMENT

We are grateful to Ruth M. Mandel and Jaehwan Kim (Cornell University) for editorial assistance during the preparation of this manuscript. We would also like to acknowledge Tyler J. Azbell and Sean M. Griffin (Cornell University) for assistance with sample preparation during the course of the TRPL measurements.

Funding Sources

The initial development of photoactive materials with potential applications in heterogeneous photocatalysis and biological sensing was supported by the National Institute of General Medical Sciences of the National Institutes of Health under award number R35GM138165 (A.H., J.J.F.R., T.A.P., P.J.M.). The content is solely the responsibility of the authors and does not necessarily represent the official views of the National Institutes of Health. Further support was provided by a Cornell University College of Arts and Sciences New Frontiers Grant awarded to P.J.M. and A.J.M. A.J.M. acknowledges the donors of the American Chemical Society Petroleum Research Fund for partial support of this research. This work made use of the Cornell Center for Materials Research Shared Facilities, which are supported through the NSF MRSEC program (DMR-1719875). Some of the solution-state NMR spectra in this work were collected on a Bruker INOVA 500 MHZ spectrometer that was purchased with support from the National Science Foundation (CHE-1531632).

REFERENCES

(1). Ma L; Feng X; Wang S; Wang B Recent Advances in AIEgen-Based Luminescent Metal–Organic Frameworks and Covalent Organic Frameworks. Mater. Chem. Front 2017, 1 (12), 2474–2486. 10.1039/C7QM00254H.

(2). Strieth-Kalthoff F; James MJ; Teders M; Pitzer L; Glorius F Energy Transfer Catalysis Mediated by Visible Light: Principles, Applications, Directions. Chem. Soc. Rev 2018, 47 (19), 7190–7202. 10.1039/C8CS00054A. [PubMed: 30088504]

(3). Romero NA; Nicewicz DA Organic Photoredox Catalysis. Chem. Rev 2016, 116 (17), 10075–10166. 10.1021/acs.chemrev.6b00057. [PubMed: 27285582]

(4). Boens N; Leen V; Dehaen W Fluorescent Indicators Based on BODIPY. Chem. Soc. Rev 2012, 41 (3), 1130–1172. 10.1039/C1CS15132K. [PubMed: 21796324]

(5). Sarkar D; Pramanik AK; Mondal TK Coumarin Based Dual Switching Fluorescent ‘Turn-on’ Chemosensor for Selective Detection of Zn^{2+} and HSO_4^-: An Experimental and Theoretical Study. RSC Adv. 2014, 4 (48), 25341–25347. 10.1039/C4RA02765E.

(6). S K; Sam B; George L; N SY; Varghese A Fluorescein Based Fluorescence Sensors for the Selective Sensing of Various Analytes. J. Fluoresc 2021, 31 (5), 1251–1276. 10.1007/s10895-021-02770-9. [PubMed: 34255257]

(7). Chern M; Kays JC; Bhuckory S; Dennis AM Sensing with Photoluminescent Semiconductor Quantum Dots. Methods Appl. Fluoresc 2019, 7 (1), 012005. 10.1088/2050-6120/aaf6f8. [PubMed: 30530939]

(8). Chan C-Y; Tanaka M; Lee Y-T; Wong Y-W; Nakanotani H; Hatakeyama T; Adachi C Stable Pure-Blue Hyperfluorescence Organic Light-Emitting Diodes with High-Efficiency and Narrow Emission. Nat. Photonics 2021, 15 (3), 203–207. 10.1038/s41566-020-00745-z.

(9). Gutiérrez M; Zhang Y; Tan J-C Confinement of Luminescent Guests in Metal–Organic Frameworks: Understanding Pathways from Synthesis and Multimodal Characterization to Potential Applications of LG@MOF Systems. Chem. Rev 2022, 122 (11), 10438–10483. 10.1021/acs.chemrev.1c00980. [PubMed: 35427119]

(10). Zhu L; Zhu B; Luo J; Liu B Design and Property Modulation of Metal–Organic Frameworks with Aggregation-Induced Emission. ACS Materials Lett. 2021, 3 (1), 77–89. 10.1021/acsmaterialslett.0c00477.

(11). Mehmood T; Reddy JP Chapter Seven - AIE-MOF Materials for Biological Applications. In Progress in Molecular Biology and Translational Science; Bhosale RS, Singh V, Eds.; Advances in Aggregation Induced Emission Materials in Biosensing and Imaging for Biomedical Applications - Part B; Academic Press, 2021; Vol. 185, pp 179–198. 10.1016/bs.pmbts.2021.06.013. [PubMed: 34782104]

(12). Leith GA; Martin CR; Mayers JM; Kittikhunnatham P; Larsen RW; Shustova NB Confinement-Guided Photophysics in MOFs, COFs, and Cages. Chem. Soc. Rev 2021, 50 (7), 4382–4410. 10.1039/D0CS01519A. [PubMed: 33594994]

(13). Rice AM; Martin CR; Galitskiy VA; Berseneva AA; Leith GA; Shustova NB Photophysics Modulation in Photoswitchable Metal–Organic Frameworks. Chem. Rev 2020, 120 (16), 8790–8813. 10.1021/acs.chemrev.9b00350. [PubMed: 31638383]

(14). Zhuang Z; Liu D Conductive MOFs with Photophysical Properties: Applications and Thin-Film Fabrication. Nano-Micro Lett. 2020, 12 (1), 132. 10.1007/s40820-020-00470-w.

(15). Dolgopolova EA; Rice AM; Martin CR; Shustova NB Photochemistry and Photophysics of MOFs: Steps towards MOF-Based Sensing Enhancements. Chem. Soc. Rev 2018, 47 (13), 4710–4728. 10.1039/C7CS00861A. [PubMed: 29546889]

(16). Dong J; Shen P; Ying S; Li Z-J; Yuan YD; Wang Y; Zheng X; Peh SB; Yuan H; Liu G; Cheng Y; Pan Y; Shi L; Zhang J; Yuan D; Liu B; Zhao Z; Tang BZ; Zhao D Aggregation-Induced Emission-Responsive Metal–Organic Frameworks. Chem. Mater 2020, 32 (15), 6706–6720. 10.1021/acs.chemmater.0c02277.

(17). Shustova NB; Ong T-C; Cozzolino AF; Michaelis VK; Griffin RG; Dincă M Phenyl Ring Dynamics in a Tetraphenylethylene-Bridged Metal-Organic Framework: Implications for the Mechanism of Aggregation-Induced Emission. J Am Chem Soc 2012, 134 (36), 15061–15070. 10.1021/ja306042w. [PubMed: 22889020]

(18). Shustova NB; McCarthy BD; Dincă M Turn-On Fluorescence in Tetraphenylethylene-Based Metal–Organic Frameworks: An Alternative to Aggregation-Induced Emission. J. Am. Chem. Soc 2011, 133 (50), 20126–20129. 10.1021/ja209327q. [PubMed: 22074054]

(19). Bauer CA; Timofeeva TV; Settersten TB; Patterson BD; Liu VH; Simmons BA; Allendorf MD Influence of Connectivity and Porosity on Ligand-Based Luminescence in Zinc Metal–Organic Frameworks. J. Am. Chem. Soc 2007, 129 (22), 7136–7144. 10.1021/ja0700395. [PubMed: 17503820]

(20). Ajoyan Z; Mandl GA; Donnarumma PR; Quezada-Novoa V; Bicalho A; Titi HM; Capobianco JA; Howarth AJ Modulating Photo- and Radioluminescence in Tb(III) Cluster-Based Metal–Organic Frameworks. ACS Mater. Lett 2022, 4 (6), 1025–1031. 10.1021/acsmaterialslett.2c00099.

(21). Yang L; Dou Y; Qin L; Chen L; Xu M; Kong C; Zhang D; Zhou Z; Wang S A Lanthanide-Containing Coordination Polymer Using Tetraphenylethene-Based Linkers with Selective Fe^{3+} Sensing and Efficient Iodine Adsorption Activities. Inorg. Chem 2020, 59 (22), 16644–16653. 10.1021/acs.inorgchem.0c02604. [PubMed: 33151057]

(22). Hu F; Di Z; Lin P; Huang P; Wu M; Jiang F; Hong M An Anionic Uranium-Based Metal–Organic Framework with Ultralarge Nanocages for Selective Dye Adsorption. Cryst. Growth Des 2018, 18 (2), 576–580. 10.1021/acs.cgd.7b01525.

(23). Gu SF; Xiong XH; Gong LL; Zhang HP; Xu Y; Feng XF; Luo F Classified Encapsulation of an Organic Dye and Metal–Organic Complex in Different Molecular Compartments for White-Light Emission and Selective Adsorption of C_2H_2 over CO_2. Inorg. Chem 2021, 60 (11), 8211–8217. 10.1021/acs.inorgchem.1c00863. [PubMed: 34018393]

(24). Huai R; Xu M; Dou Y; Wang Z; Xue Z; Zhang Y; Lv H; Qin L; Zhang D; Zhou Z; Yang L Synthesis of a Tetraphenylethylene-Based Metal-Organic Framework as the Luminescent Sensor for Selective Sensing of $Cr_2O_7^{2-}$ in Aqueous Solution. Inorg. Chem. Commun 2021, 127, 108550. 10.1016/j.inoche.2021.108550.

(25). Wu X-X; Fu H-R; Han M-L; Zhou Z; Ma L-F Tetraphenylethylene Immobilized Metal–Organic Frameworks: Highly Sensitive Fluorescent Sensor for the Detection of $Cr_2O_7^{2-}$ and Nitroaromatic Explosives. Cryst. Growth Des 2017, 17 (11), 6041–6048. 10.1021/acs.cgd.7b01155.

(26). Chen FE; Pitt TA; Okong'o DJ; Wetherbee LG; Fuentes-Rivera JJ; Milner PJ A Structure–Activity Study of Aromatic Acid Modulators for the Synthesis of Zirconium-Based Metal–Organic Frameworks. Chem. Mater 2022, 34 (7), 3383–3394. 10.1021/acs.chemmater.2c00241. [PubMed: 36238710]

(27). Forgan RS Modulated Self-Assembly of Metal–Organic Frameworks. Chem. Sci 2020, 11 (18), 4546–4562. 10.1039/D0SC01356K. [PubMed: 34122913]

(28). Atzori C; Shearer GC; Maschio L; Civalleri B; Bonino F; Lamberti C; Svelle S; Lillerud KP; Bordiga S Effect of Benzoic Acid as a Modulator in the Structure of UiO-66: An Experimental and Computational Study. J. Phys. Chem. C 2017, 121 (17), 9312–9324. 10.1021/acs.jpcc.7b00483.

(29). Shearer GC; Vitillo JG; Bordiga S; Svelle S; Olsbye U; Lillerud KP Functionalizing the Defects: Postsynthetic Ligand Exchange in the Metal Organic Framework UiO-66. Chem. Mater 2016, 28 (20), 7190–7193. 10.1021/acs.chemmater.6b02749.

(30). Shearer GC; Chavan S; Bordiga S; Svelle S; Olsbye U; Lillerud KP Defect Engineering: Tuning the Porosity and Composition of the Metal–Organic Framework UiO-66 via Modulated Synthesis. Chem. Mater 2016, 28 (11), 3749–3761. 10.1021/acs.chemmater.6b00602.

(31). Fang Z; Bueken B; De Vos DE; Fischer RA Defect-Engineered Metal–Organic Frameworks. Angew. Chem. Int. Ed 2015, 54 (25), 7234–7254. 10.1002/anie.201411540.

(32). Gutov OV; Hevia MG; Escudero-Adán EC; Shafir A Metal–Organic Framework (MOF) Defects under Control: Insights into the Missing Linker Sites and Their Implication in the Reactivity of Zirconium-Based Frameworks. Inorg. Chem 2015, 54 (17), 8396–8400. 10.1021/acs.inorgchem.5b01053. [PubMed: 26291237]

(33). Shearer GC; Chavan S; Ethiraj J; Vitillo JG; Svelle S; Olsbye U; Lamberti C; Bordiga S; Lillerud KP Tuned to Perfection: Ironing Out the Defects in Metal–Organic Framework UiO-66. Chem. Mater 2014, 26 (14), 4068–4071. 10.1021/cm501859p.

(34). Øien S; Wragg D; Reinsch H; Svelle S; Bordiga S; Lamberti C; Lillerud KP Detailed Structure Analysis of Atomic Positions and Defects in Zirconium Metal–Organic Frameworks. Cryst. Growth Des 2014, 14 (11), 5370–5372. 10.1021/cg501386j.

(35). Wu H; Chua YS; Krungleviciute V; Tyagi M; Chen P; Yildirim T; Zhou W Unusual and Highly Tunable Missing-Linker Defects in Zirconium Metal–Organic Framework UiO-66 and Their Important Effects on Gas Adsorption. J. Am. Chem. Soc 2013, 135 (28), 10525–10532. 10.1021/ja404514r. [PubMed: 23808838]

(36). Schaate A; Roy P; Godt A; Lippke J; Waltz F; Wiebcke M; Behrens P Modulated Synthesis of Zr-Based Metal–Organic Frameworks: From Nano to Single Crystals. Chem. Eur. J 2011, 17 (24), 6643–6651. 10.1002/chem.201003211. [PubMed: 21547962]

(37). Cavka JH; Jakobsen S; Olsbye U; Guillou N; Lamberti C; Bordiga S; Lillerud KP A New Zirconium Inorganic Building Brick Forming Metal Organic Frameworks with Exceptional Stability. J. Am. Chem. Soc 2008, 130 (42), 13850–13851. 10.1021/ja8057953. [PubMed: 18817383]

(38). Bai Y; Dou Y; Xie L-H; Rutledge W; Li J-R; Zhou H-C Zr-Based Metal–Organic Frameworks: Design, Synthesis, Structure, and Applications. Chem. Soc. Rev 2016, 45 (8), 2327–2367. 10.1039/C5CS00837A. [PubMed: 26886869]

(39). Dhakshinamoorthy A; Alvaro M; Horcajada P; Gibson E; Vishnuvarthan M; Vimont A; Grenèche J-M; Serre C; Daturi M; Garcia H Comparison of Porous Iron Trimesates Basolite F300 and MIL-100(Fe) As Heterogeneous Catalysts for Lewis Acid and Oxidation Reactions: Roles of Structural Defects and Stability. ACS Catal. 2012, 2 (10), 2060–2065. 10.1021/cs300345b.

(40). Taddei M; Schukraft GM; Warwick MEA; Tiana D; McPherson MJ; Jones DR; Petit C Band Gap Modulation in Zirconium-Based Metal–Organic Frameworks by Defect Engineering. J. Mater. Chem. A 2019, 7 (41), 23781–23786. 10.1039/C9TA05216J.

(41). Rouillon J; Monnereau C; Andraud C Reevaluating the Solution Photophysics of Tetraphenylethylene at the Origin of Their Aggregation-Induced Emission Properties. Chem. Eur. J 2021, 27 (30), 8003–8007. 10.1002/chem.202100926. [PubMed: 33769628]

(42). Kokado K; Sada K Consideration of Molecular Structure in the Excited State to Design New Luminogens with Aggregation-Induced Emission. Angew. Chem. Int. Ed 2019, 58 (26), 8632–8639. 10.1002/anie.201814462.

(43). Zhang H; Zhao Z; Turley AT; Wang L; McGonigal PR; Tu Y; Li Y; Wang Z; Kwok RTK; Lam JWY; Tang BZ Aggregate Science: From Structures to Properties. Adv. Mater 2020, 32 (36), 2001457. 10.1002/adma.202001457.

(44). Suzuki S; Sasaki S; Sairi AS; Iwai R; Tang BZ; Konishi G Principles of Aggregation-Induced Emission: Design of Deactivation Pathways for Advanced AIEgens and Applications. Angew. Chem 2020, 132 (25), 9940–9951. 10.1002/ange.202000940.

(45). Huang S; Ding J; Bi A; Yu K; Zeng W Insights into Optical Probes Based on Aggregation-Induced Emission: From Restriction of Intramolecular Motions to Dark State. Adv. Opt. Mater 2021, 9 (21), 2100832. 10.1002/adom.202100832.

(46). Li Z-J; Wang X; Zhu L; Ju Y; Wang Z; Zhao Q; Zhang Z-H; Duan T; Qian Y; Wang J-Q; Lin J Hydrolytically Stable Zr-Based Metal–Organic Framework as a Highly Sensitive and Selective Luminescent Sensor of Radionuclides. Inorg. Chem 2022, 61 (19), 7467–7476. 10.1021/acs.inorgchem.2c00545. [PubMed: 35514048]

(47). Bon V; Senkovska I; Weiss MS; Kaskel S Tailoring of Network Dimensionality and Porosity Adjustment in Zr- and Hf-Based MOFs. CrystEngComm 2013, 15 (45), 9572. 10.1039/c3ce41121d.

(48). Addicoat MA; Coupry DE; Heine T AuToGraFS: Automatic Topological Generator for Framework Structures. J. Phys. Chem. A 2014, 118 (40), 9607–9614. 10.1021/jp507643v. [PubMed: 25208338]

(49). Addicoat MA; Vankova N; Akter IF; Heine T Extension of the Universal Force Field to Metal–Organic Frameworks. J. Chem. Theory Comput 2014, 10 (2), 880–891. 10.1021/ct400952t. [PubMed: 26580059]

(50). Coupry DE; Addicoat MA; Heine T Extension of the Universal Force Field for Metal–Organic Frameworks. J. Chem. Theory Comput 2016, 12 (10), 5215–5225. 10.1021/acs.jctc.6b00664. [PubMed: 27580382]

(51). Amsterdam Modeling Suite Making Computational Chemistry Work For You. Software for Chemistry & Materials. https://www.scm.com/ (accessed 2022-04-28).

(52). Zhang Q; Su J; Feng D; Wei Z; Zou X; Zhou H-C Piezofluorochromic Metal–Organic Framework: A Microscissor Lift. J. Am. Chem. Soc 2015, 137 (32), 10064–10067. 10.1021/jacs.5b04695. [PubMed: 26214704]

(53). J. Garibay S; K. Farha O; B. DeCoste J Single-Component Frameworks for Heterogeneous Catalytic Hydrolysis of Organophosphorous Compounds in Pure Water. Chem. Commun 2019, 55 (49), 7005–7008. 10.1039/C9CC02236H.

(54). Wei Z; Gu Z-Y; Arvapally RK; Chen Y-P; McDougald RN; Ivy JF; Yakovenko AA; Feng D; Omary MA; Zhou H-C Rigidifying Fluorescent Linkers by Metal–Organic Framework Formation for Fluorescence Blue Shift and Quantum Yield Enhancement. J. Am. Chem. Soc 2014, 136 (23), 8269–8276. 10.1021/ja5006866. [PubMed: 24819882]

(55). Schubert U Clusters with a Zr_6O_8 Core. Coord. Chem. Rev 2022, 469, 214686. 10.1016/j.ccr.2022.214686.

(56). Zhang J-W; Li H; Li J-Q; Chen Y; Qu P; Zhai Q-G Enhancement of the Fluorescence Properties via Introducing the Tetraphenylethylene Chromophores into a Novel Mn–Organic Framework with a Rare $[Mn_4(M_3\text{-}OH)_2]$ Cluster. Dalton Trans. 2021, 50 (47), 17482–17486. 10.1039/D1DT03349B. [PubMed: 34788353]

(57). Sohail M; Altaf M; Baig N; Jamil R; Sher M; Fazal A A New Water Stable Zinc Metal Organic Framework as an Electrode Material for Hydrazine Sensing. New J. Chem 2018, 42 (15), 12486–12491. 10.1039/C8NJ01507D.

(58). Lei M; Ge F; Gao X; Shi Z; Zheng H A Water-Stable Tb-MOF As a Rapid, Accurate, and Highly Sensitive Ratiometric Luminescent Sensor for the Discriminative Sensing of Antibiotics and D_2O in H_2O. Inorg. Chem 2021, 60 (14), 10513–10521. 10.1021/acs.inorgchem.1c01145. [PubMed: 34170146]

(59). Yu H; Fan M; Liu Q; Su Z; Li X; Pan Q; Hu X Two Highly Water-Stable Imidazole-Based Ln-MOFs for Sensing Fe^{3+},$Cr_2O_7^{2-}$/CrO_4^{2-} in a Water Environment. Inorg. Chem 2020, 59 (3), 2005–2010. 10.1021/acs.inorgchem.9b03364. [PubMed: 31935076]

(60). Pattengale B; Ostresh S; Schmuttenmaer CA; Neu J Interrogating Light-Initiated Dynamics in Metal–Organic Frameworks with Time-Resolved Spectroscopy. Chem. Rev 2022, 122 (1), 132–166. 10.1021/acs.chemrev.1c00528. [PubMed: 34613710]

(61). Cerasale DJ; Ward DC; Easun TL MOFs in the Time Domain. Nat. Rev. Chem 2022, 6 (1), 9–30. 10.1038/s41570-021-00336-8.

(62). Electronic Processes in Organic Semiconductors: An Introduction | Wiley. Wiley.com. https://www.wiley.com/en-us/Electronic+Processes+in+Organic+Semiconductors%3A+An+Introduction-p-9783527332922 (accessed 2022-05-24).

(63). Herz LM; Silva C; Grimsdale AC; Müllen K; Phillips RT Time-Dependent Energy Transfer Rates in a Conjugated Polymer Guest-Host System. Phys. Rev. B 2004, 70 (16), 165207. 10.1103/PhysRevB.70.165207.

(64). Meskers SCJ; Hübner J; Oestreich M; Bässler H Dispersive Relaxation Dynamics of Photoexcitations in a Polyfluorene Film Involving Energy Transfer: Experiment and Monte Carlo Simulations. J. Phys. Chem. B 2001, 105 (38), 9139–9149. 10.1021/jp0113331.

(65). Kennedy SP; Garro N; Phillips RT Time-Resolved Site-Selective Spectroscopy of Poly (p-Phenylene Vinylene). Phys. Rev. B 2001, 64 (11), 115206. 10.1103/PhysRevB.64.115206.

(66). Rauscher U; Bässler H; Bradley DDC; Hennecke M Exciton versus Band Description of the Absorption and Luminescence Spectra in Poly(*p*-Phenylenevinylene). Phys. Rev. B 1990, 42 (16), 9830–9836. 10.1103/PhysRevB.42.9830.

(67). Prasad PN; Morgan JR; El-Sayed MA Spectral Diffusion in Orientationally Disordered Organic Solids. J. Phys. Chem 1981, 85 (24), 3569–3571. 10.1021/j150624a009.

(68). Lakowicz JR Principles of Fluorescence Spectroscopy, 3rd ed.; Springer: New York, 2006.

(69). Nishida J; Tamimi A; Fei H; Pullen S; Ott S; Cohen SM; Fayer MD Structural Dynamics inside a Functionalized Metal–Organic Framework Probed by Ultrafast 2D IR Spectroscopy. Proc. Natl. Acad. Sci. USA 2014, 111 (52), 18442–18447. 10.1073/pnas.1422194112. [PubMed: 25512539]

(70). Albrecht C Lakowicz Joseph R.: Principles of Fluorescence Spectroscopy, 3rd Edition. Anal. Bioanal. Chem 2008, 390 (5), 1223–1224. 10.1007/s00216-007-1822-x.

(71). Guan J; Wei R; Prlj A; Peng J; Lin K-H; Liu J; Han H; Corminboeuf C; Zhao D; Yu Z; Zheng J Direct Observation of Aggregation-Induced Emission Mechanism. Angew. Chem 2020, 132 (35), 15013–15019. 10.1002/ange.202004318.

(72). Musser AJ; Rajendran SK; Georgiou K; Gai L; Grant RT; Shen Z; Cavazzini M; Ruseckas A; Turnbull GA; Samuel IDW; Clark J; Lidzey DG Intermolecular States in Organic Dye Dispersions: Excimers vs. Aggregates. J. Mater. Chem. C 2017, 5 (33), 8380–8389. 10.1039/C7TC02655B.

(73). Haldar R; Jakoby M; Mazel A; Zhang Q; Welle A; Mohamed T; Krolla P; Wenzel W; Diring S; Odobel F; Richards BS; Howard IA; Wöll C Anisotropic Energy Transfer in Crystalline Chromophore Assemblies. Nat. Commun 2018, 9 (1), 4332. 10.1038/s41467-018-06829-3. [PubMed: 30337528]

(74). Cao L; Lin Z; Shi W; Wang Z; Zhang C; Hu X; Wang C; Lin W Exciton Migration and Amplified Quenching on Two-Dimensional Metal–Organic Layers. J. Am. Chem. Soc 2017, 139 (20), 7020–7029. 10.1021/jacs.7b02470. [PubMed: 28467852]

(75). Corradi G; Krampf A; Messerschmidt S; Vittadello L; Imlau M Excitonic Hopping-Pinning Scenarios in Lithium Niobate Based on Atomistic Models: Different Kinds of Stretched Exponential Kinetics in the Same System. J. Phys. Condens. Matter 2020, 32 (41), 413005. 10.1088/1361-648X/ab9c5b. [PubMed: 32531769]

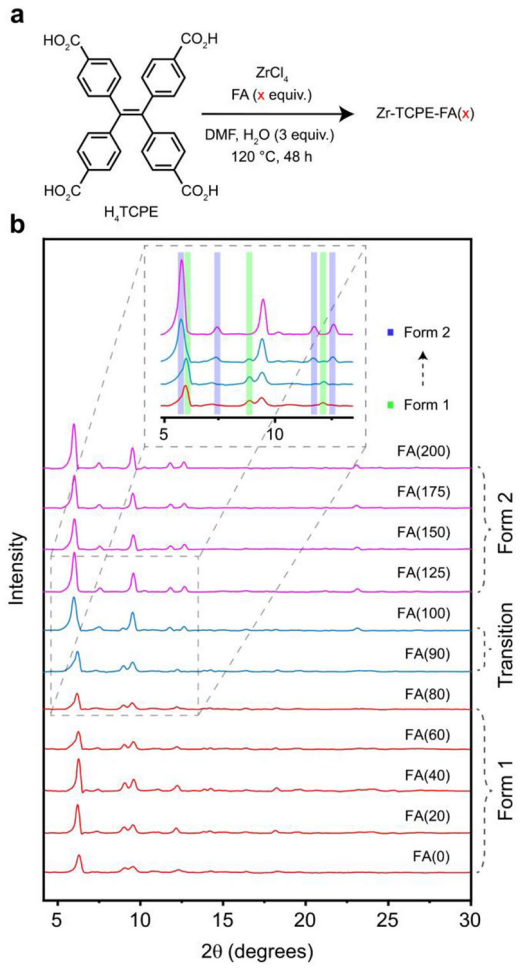

Figure 1.

a) Synthesis of Zr-TCPE-FA(x) from H_4TCPE and $ZrCl_4$; x = equivalents of FA used compared to H_4TCPE. b) PXRD patterns of Zr-TCPE-FA(x) samples, with Form 1 (red, FA(0) to FA(80)), transition from Form 1 to Form 2 (cyan, FA(90) to FA(100)), and Form 2 (pink, FA(125) to FA(200)) indicated. Inset: Transition from Form 1 to Form 2. The experimental PXRD patterns were baseline-corrected.

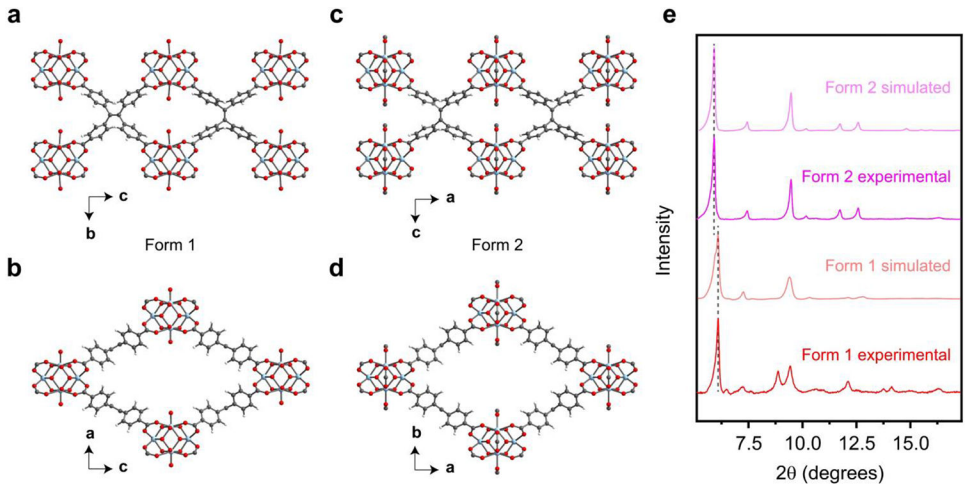

Figure 2.

Simulated structures of Form 1 viewing along *a* (a) and *b* (b) and of Form 2 viewing along *b* (c) and *c* (d) of Zr-TCPE with **scu** topology. e) Comparison of the simulated and experimental PXRD patterns corresponding to Form 1 and Form 2 of Zr-TCPE MOFs with **scu** topology. The experimental PXRD patterns were baseline-corrected.

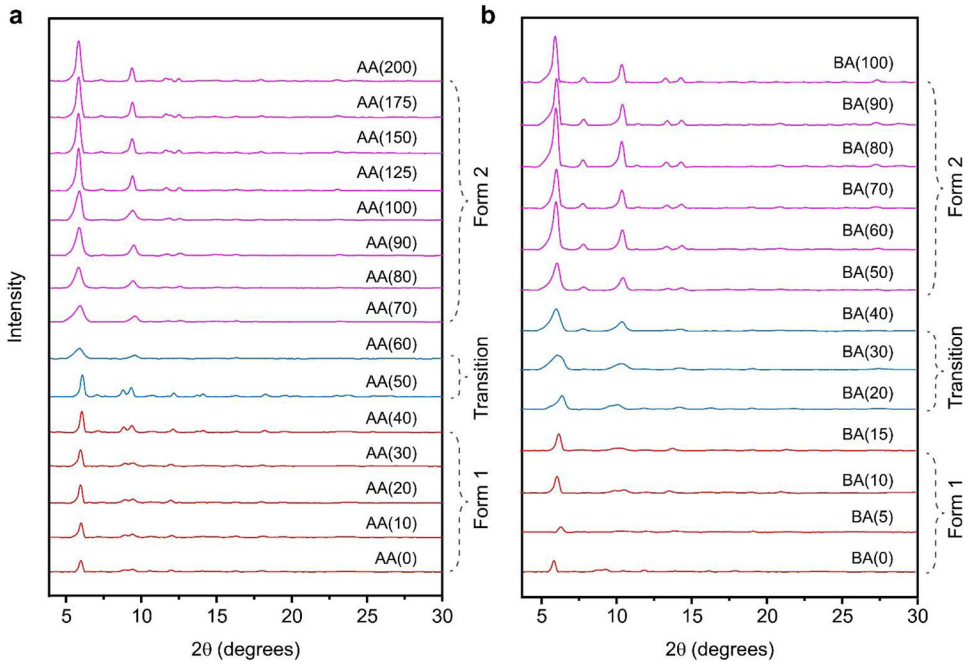

Figure 3.

Form switching in Zr-TCPE-AA(x) and Zr-TCPE-BA(x) MOFs; x = equivalents of AA or BA used compared to H_4TCPE. a) PXRD patterns of Zr-TCPE-AA(x) samples, with Form 1 (red, AA(0) to AA(40)), transition from Form 1 to Form 2 (cyan, AA(50) to AA(60)), and Form 2 (pink, AA(70) to AA(200)) indicated. b) PXRD patterns of Zr-TCPE-BA(x) samples, with Form 1 (red, BA(0) to BA(15)), transition from Form 1 to Form 2 (cyan, BA(20) to BA(40)), and Form 2 (pink, BA(50) to BA(100)) indicated. The experimental PXRD patterns were baseline-corrected.

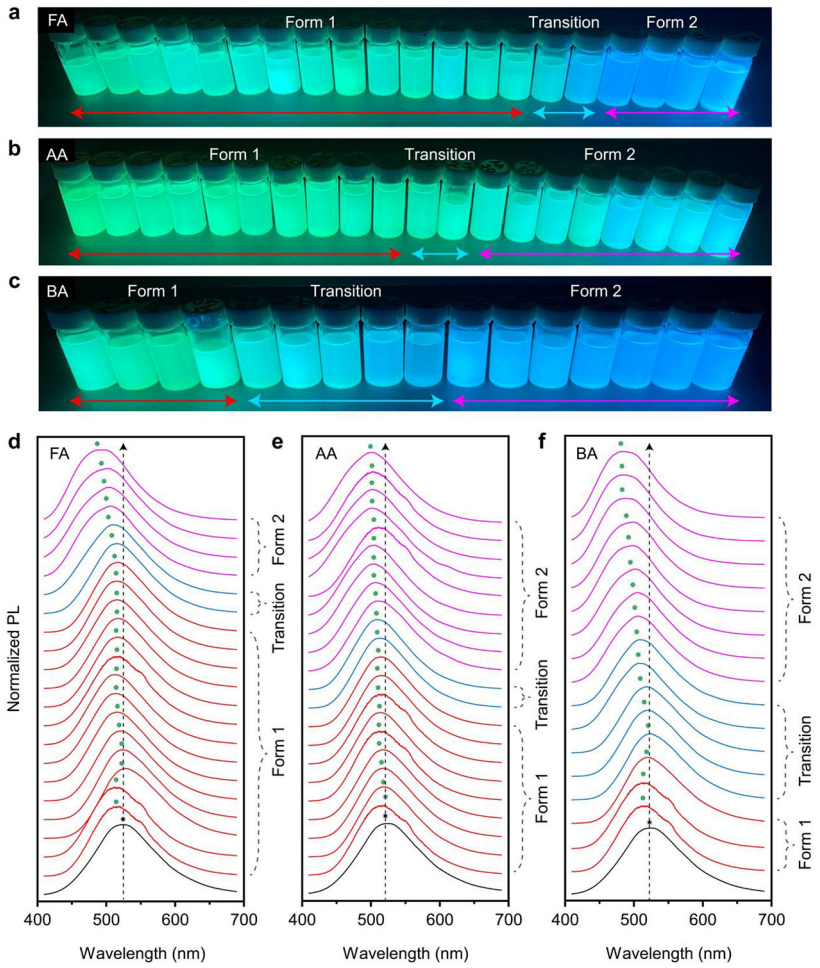

Figure 4.

a-c) Images of Zr-TCPE samples suspended in dichloromethane and irradiated with UV light. The phase transitions observed by PXRD are indicated with double-headed arrows. PL spectra for d) Zr-TCPE-FA(x) and e) Zr-TCPE-AA(x), respectively, where x = 0, 5, 10, 15, 20, 25, 30, 35, 35, 40, 45, 50, 60, 70, 80, 90, 100, 125, 150, 175, 200. f) PL spectra for Zr-TCPE-BA(x), where x = 0, 5, 10, 15, 20, 25, 30, 35, 40, 45, 50, 60, 70, 80, 90, 100. The PL spectrum of H_4TCPE is included for reference (black). The PL spectra are color-coded based on the PXRD data for each sample, with Form 1 (red), Form 2 (pink), and mixtures of phases (cyan) indicated. Dotted lines correspond to the PL maximum of H_4TCPE, and green stars represent the PL maxima of each sample.

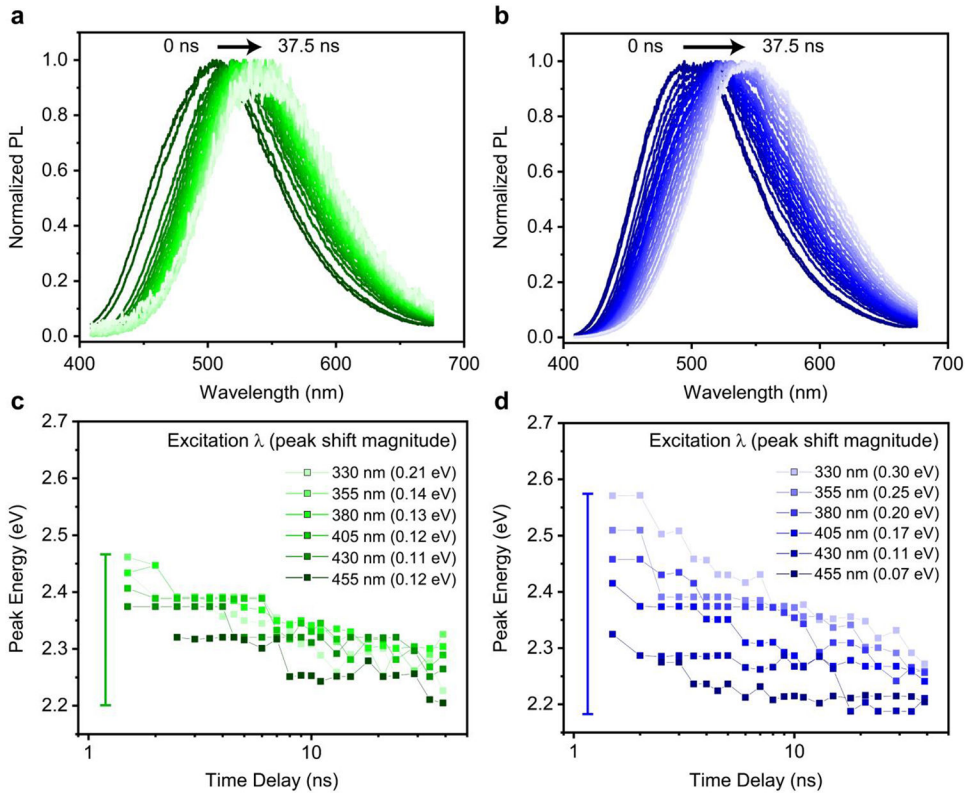

Figure 5.

Monitoring spectral diffusion in a, c) Zr-TCPE-FA(50) and b, d) Zr-TCPE-FA(200), representing Form 1 and Form 2, respectively. In a) and b), PL spectral slices over the first 37.5 ns after photoexcitation at 355 nm are overlaid and normalized for clarity. The lengths of the arrows reflect the increased spectral diffusion for Form 2 compared to Form 1. The excitation wavelength-dependent peak positions over time in c) and d) are tracked via peak wavelength position and converted to an energy scale. The scale bars are added to visualize the broader density of sampled states for Form 2 compared to Form 1.

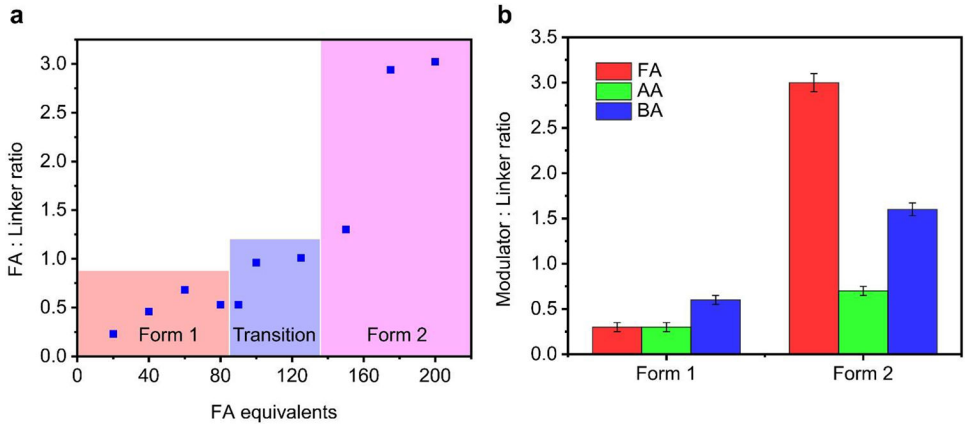

Figure 6.

a) Formate:$TCPE^{4-}$ ratios in Zr-TCPE-FA(x) samples, as determined by ^{1}H NMR after digestion with K_3PO_4/D_2O. b) Formate:$TCPE^{4-}$, acetate:$TCPE^{4-}$, and benzoate:$TCPE^{4-}$ ratios in representative Zr-TCPE samples of Form 1 (Zr-TCPE-FA(50), Zr-TCPE-AA(35), Zr-TCPE-BA(5)) and Form 2 (Zr-TCPE-FA(200), Zr-TCPE-AA(100), Zr-TCPE-BA(100)), as determined by ^{1}H NMR after digestion with K_3PO_4/D_2O.